Title: *Distinct signatures of reward value and variance on spiking activity and functional interactions in monkey fronto-parietal areas*

Authors: Bahareh Taghizadeh[1*], Saeed Karimimehr[1*], Nicholas C. Foley[2,3*], Michael Cohanpour[2,3], Mulugeta Semework[2,3], Sameer A. Sheth[4], Reza Lashgari[1] and Jacqueline Gottlieb[2,3,5]

*Equal contribution

Author affiliation: [1]Brain Engineering Research Lab, School of Cognitive Sciences, Institute for Research in Fundamental Sciences, Tehran 19395-5746, Iran, [2]Department of Neuroscience, [3]Zuckerman Mind Brain Behavior Institute, Columbia University, [4]Department of Neurosurgery, Baylor College of Medicine, [5]The Kavli Institute for Brain Science, Columbia University

Corresponding author:

Jacqueline Gottlieb, PhD
Department of Neuroscience
Columbia University
3227 Broadway,
New York, NY 10025
E-mail: jg2141@columbia.edu

Number of figures: 8

Acknowledgements: The work was supported by a generous gift from Synthes, Inc. and a McKnight Foundation Memory and Cognitive Disorder Award to JG.

Author Contributions: NCF and JG designed the experiment. NCF, SAS, MC, MS and JG implemented the experiment and collected the data. BT, SK, RL and JG analyzed the data and wrote the manuscript.

Disclosure statement:

The authors declare that they have no conflict of interest.

Abstract

The expected value (EV) and uncertainty of reward distributions have widespread effects on behavior and neural activity, but their effects on cognitive functions are poorly understood. Here we show that EV and uncertainty have dissociable effects on monkey frontal and parietal areas implicated in executive function. Uncertainty and EV were encoded by distinct populations of cells in each area, and they differentially modulated within- and across-area information transmission. EV enhanced the coherence between spikes and local field potential (SFC) within the frontal and the parietal lobe, suggesting that it enhanced within-area information transmission. In contrast, uncertainty enhanced parietal to frontal SFC but suppressed SFC in the top-down direction, suggesting that it selectively enhanced information transmission from the parietal to the frontal lobe. The results reveal cellular mechanisms through which reward and uncertainty can independently modulate executive function and support a primary role for the parietal cortex in processing information under uncertainty.

Introduction

Forming accurate expectations of uncertain rewards is essential for adaptive behavior in changing conditions. Reward-related neural activity, including responses to the average (expected) value (EV) and variance (uncertainty) of reward distributions have been intensively investigated and shown to modulate activity in many parts of the brain[1, 2]. However, in addition to modulating action decisions, reward expectations shape cognitive processes such as attention and executive function, but the effects of rewards on cognitive control are less well understood[3, 4].

According to the expected value of control (EVC) theory, the interface between valuation and executive function involves interacting processes of *monitoring* and *regulation*[5]. A general-purpose valuation network relying heavily on the anterior cingulate cortex (ACC) monitors the value of a task and the level of attention or cognitive effort that is desirable to allocate to the task. A separate network of dorsal frontal and parietal areas plays a regulatory role, implementing the attentional policy specified by the ACC. However, while the EVC theory is supported by converging evidence in rodents and the human brain [6-9], the cellular effects of reward and uncertainty in the monkey fronto-parietal network - the primary model system for cortical attention control - remain poorly understood.

In monkeys, the regulation of attention and working memory depends on several frontal and parietal areas that are organized in circuits with distinct functional profiles and anatomical connectivity[10-13]. Two nodes of the fronto-parietal network, the frontal eye field (FEF) and lateral intraparietal area (LIP) have strong visual and oculomotor responses and are important for the moment by moment orienting of attention and gaze[14, 15]. Two additional areas, in contrast - the dorsolateral prefrontal cortex (dlPFC) and parietal area 7A - have weaker visuo-motor responses and are more sensitive to abstract variables such as short-term memory, context and rules[16, 17]. These findings suggest that the dlPFC and area 7A convey executive control, including sensitivity to incentives, for the sensorimotor orienting of attention and gaze, but important open questions remain about this hypothesis.

A first question concerns the representation of reward variables, as cells sensitive to reward-expectation have only been reported in the dlPFC[18-21] but not in 7A. It is unclear whether this difference reflects a true areal specialization or merely a gap in the empirical literature.

A second question concerns the encoding of uncertainty. While uncertainty - and specifically, risk, defined as the variance of known reward distributions - has been studied intensively in economic decisions[22], a growing literature shows that uncertainty is also a trigger for cognitive functions. Specifically, uncertainty acts as a trigger for initiating cognitive actions – such as enhanced learning rates[23] and attentional orienting[24, 25] – aimed to reduce the uncertainty. Reward uncertainty is encoded independently of expected value (EV) in dopamine cells[26], the orbitofrontal cortex[27], the anterodorsal septum[28] and the basal forebrain[29]. But it remains unknown whether, and how, it is encoded in frontal and parietal areas involved in attention regulation.

To examine these questions, we investigated the encoding of uncertainty and EV in single-neuron activity, local field potentials (LFP) and spike field connectivity (SFC) in monkey areas 7A and the dlPFC. We trained monkeys on a set of reward distributions that were signaled by familiar visual cues and independently manipulated uncertainty and EV. We show that uncertainty and EV produced distinct neural signatures in 7A and dlPFC. At the level of single-

neuron activity, uncertainty and EV were encoded by distinct populations of cells with little shared connectivity. Moreover, while EV primarily enhanced SFC within 7A and the dlPFC, suggesting that it enhanced local information transmission, uncertainty primarily modulated across-area SFC, by enhancing transmission from 7A to the dlPFC but suppressing it in the opposite direction. The results reveal cellular mechanisms through which uncertainty and EV can independently modulate executive functions, and support a specialized role of the monkey parietal cortex in processing information in conditions of uncertainty.

Results

Task and behavior

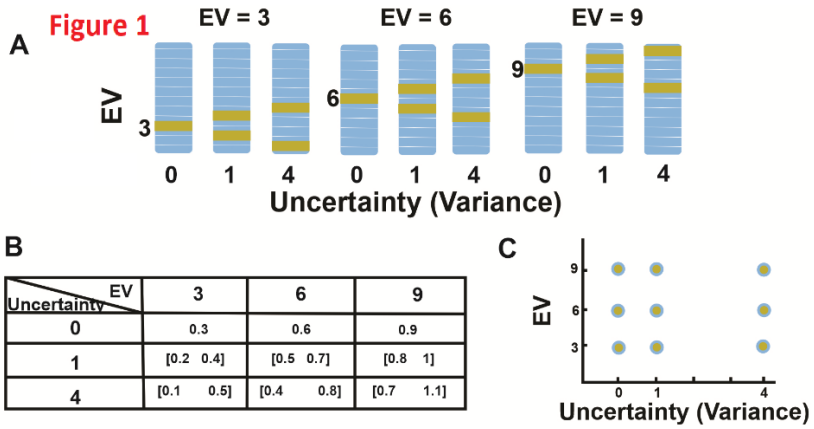

Figure 1. Reward distributions (A) Visual cues Two monkeys were familiarized with a set of 9 visual cues that signaled the possible reward magnitudes on each trial on an 11-point vertical scale (1 point = 0.1 mL of water). Three cues indicated deterministic rewards of 3, 6 or 9 points, and the remaining six cues signaled probabilistic rewards that had high or low variance around the same levels of EV. **(B) Reward magnitudes for the 9 distributions** The cues signaled unique combinations of 3 levels of EV (3, 6 or 9 points) and 3 levels of uncertainty (variance = 0 for a single reward delivered with 100% probability; variances of 1 and 4 for two equiprobable rewards symmetrically positioned around the same average EV). **(C) Orthogonalization of variance and EV** across the full set of cues.

Two monkeys performed a simple instructed-saccade task in which they formed expectations about the reward distribution that was in effect on each trial. A trial started with the presentation of a reward cue indicating the reward magnitudes that would be available for a correct response (**Fig. 1A**). Three of the cues indicated that a single reward magnitude - of respectively, 3, 6 and 9 points – would be delivered deterministically upon correct trial completion. The remaining six cues indicated that two reward magnitudes were equally likely to occur. The probabilistic rewards were symmetrically positioned around EV 3, 6 and 9 with high or low variance (uncertainty; **Fig. 1A, B**; mean-preserving spread[27]). The resulting set of 9 reward distributions statistically dissociated 3 levels of EV (3, 6 and 9 points) and 3 levels of uncertainty (reward variance of 0, 1 or 4; **Fig. 1C**). To minimize the role of learning and exploration, the monkeys were extensively familiarized with the cues before neural recordings began.

On each trial after the monkeys acquired fixation, they were shown a randomly selected reward cue and, after an additional 400 ms delay period, they were shown a saccade target and required to make a saccade to it to obtain the reward (**Fig. 2A**). The cue and the target could each fall at 8º eccentricity to the right or left of fixation and, importantly, their locations were independently randomized, so that the cues only provided information about the rewards but not the action required to obtain the rewards. This design allowed us to study the neural correlates of reward expectation independently of saccade planning or decision strategies.

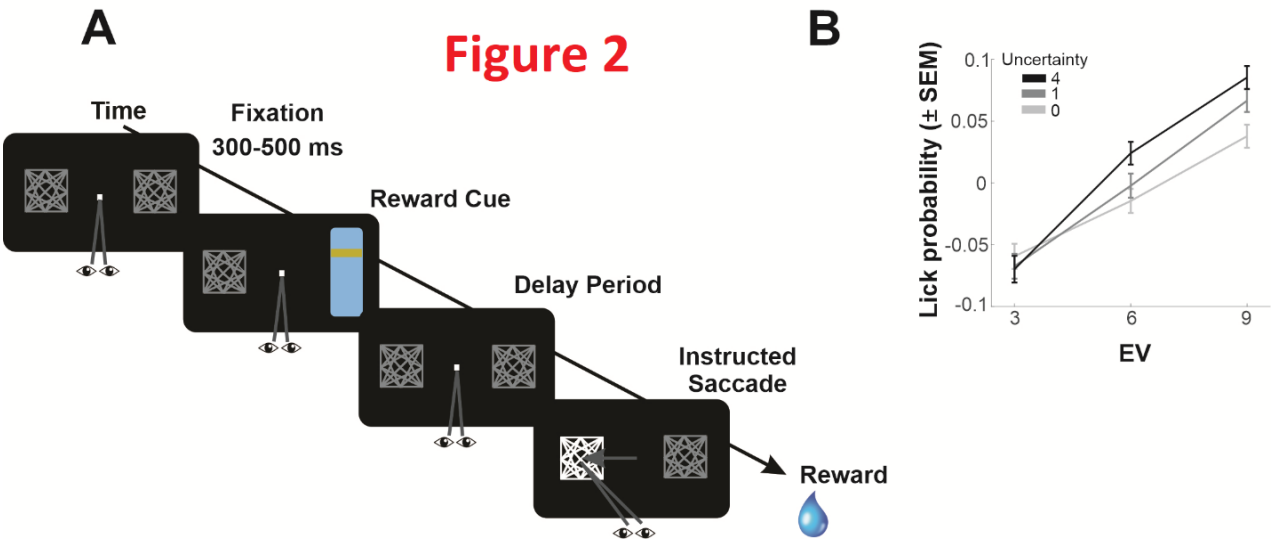

Fig. 2 Task (A) Trial events The arrow indicates time. The monkeys initiated a trial by looking at a fixation point flanked by two placeholders at 8º to the right or left of central fixation. After the initial fixation period, a randomly selected reward cue was presented for 400 ms at one of the placeholder locations. After an additional 400 ms delay (memory) period, a randomly selected placeholder increased in luminance, indicating the saccade target. If the monkeys made a saccade to the target, they received a reward according to the distribution that had been predicted by the cue. **(B) Anticipatory licking** before reward delivery increased as a function of the trial's EV and uncertainty. Points show average and SEM of the licking rates (n = 12,029 trials).

We measured the monkeys' anticipatory licking as an index of their reward expectancy. Licking probability was sensitive to both uncertainty and EV, and showed a positive interaction between the two factors whereby the effect of EV was stronger at higher levels of uncertainty (**Figure 2B**; across sessions, the mean ± SEM of GLM coefficients were, for EV: 0.24±0.002; uncertainty: 0.03±0.0006; interaction: 0.07±0.0008; all $p < 10^{-9}$ relative to 0, signed-rank test). The positive interaction between uncertainty and EV is consistent with theoretical predictions for optimal attentional allocation, and with the dual sensitivity of information seeking and oculomotor behavior to EV and uncertainty[24, 30].

To investigate the neural correlates of uncertainty and EV we implanted 50 channel "Utah" arrays in the pre-arcuate portion of the dlPFC and the caudal portion of area 7A (**Fig. S1**). We describe the effects of uncertainty and EV on LFP power and single-neuron activity, followed by their effects on spike-field coherence (SFC).

Uncertainty and EV modulate oscillatory LFP power

To examine oscillatory activity, we divided single-trial LFP traces into 1 ms bins spanning the cue and delay epochs and 1 Hz bins tiling the range of 5-50 Hz and, for each resulting 1Hz x 1 ms pixel, fit a GLM model containing uncertainty, EV, and their interaction, along with cue location to control for possible visuo-spatial effects. This resulted in a coefficient maps revealing the impact of uncertainty, EV and their interaction in this spatial-frequency range for 7A and dlPFC. This analysis showed that uncertainty and EV exerted consistent effects in two frequency bands: a lower frequency band between 8-18 Hz, corresponding to high α/low-β frequencies, and a higher band of 18-43 Hz, corresponding to the high-β/low-γ frequencies[31] (**Fig. 3**).

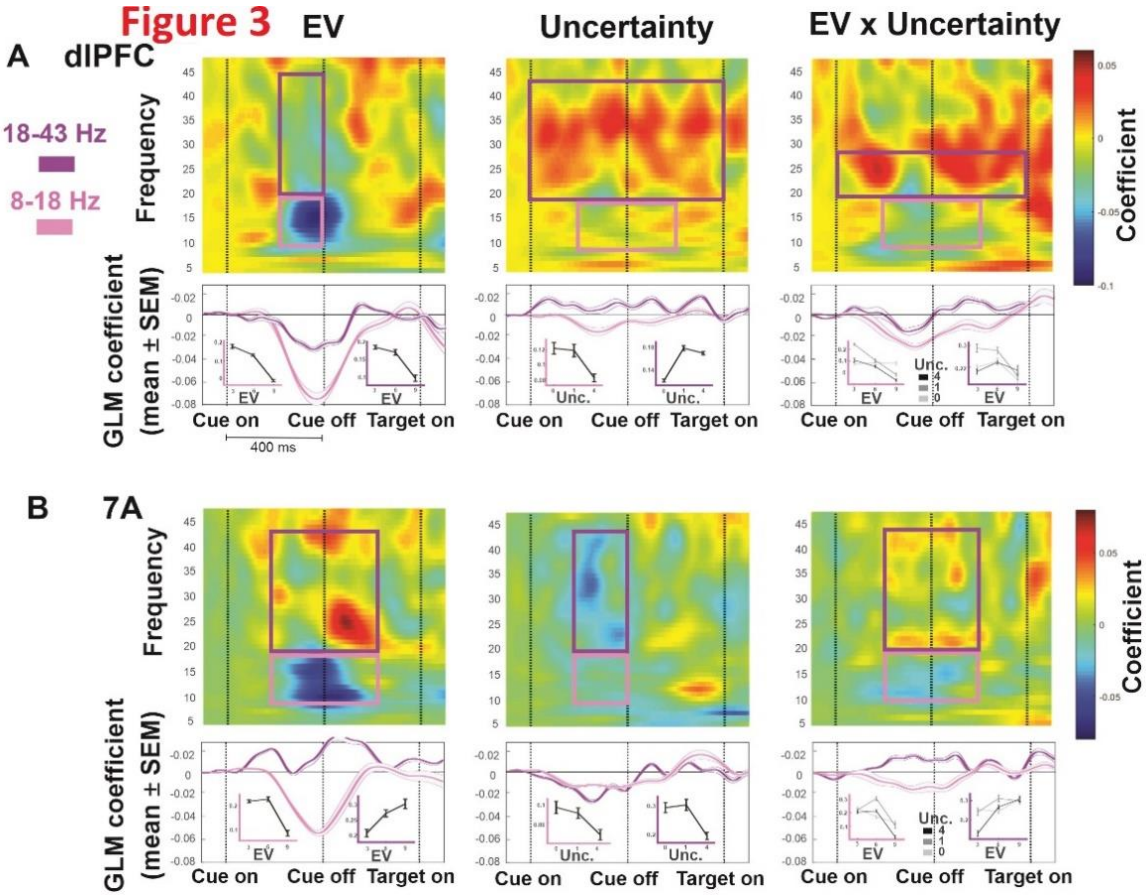

Figure 3 Effects of uncertainty and EV on LFP power (A, B) The color maps show the GLM coefficients from the dlPFC (**A**) and 7A (**B**), indicating the effects of EV, uncertainty and their interaction on LFP power as a function of frequency and time aligned on cue onset. The rectangles superimposed on each map indicate the regions of interest (ROI) in the high-α/low-β (pink) and high-β/low-Y (purple) frequency bands in which the effects were significant and consistent for both monkeys. In the panels underneath each map, the continuous traces show the average coefficient in the respective frequency band as a function of time (mean and SEM across the frequencies included in the ROI). To illustrate the data from which the coefficients were derived, the insets show the LFP power in the time-frequency ROI corresponding to the color of the axes. For these plots, z-transformed LFP power was averaged for each electrode, and the data show average and SEM across n = 48 electrodes as a function of the variable of interest (EV, uncertainty, and EV-uncertainty combinations).

The high α/low-β frequency band (8 - 18 Hz) was suppressed by uncertainty and EV in both areas, with the most consistent effects focused on the late cue and early delay periods (**Fig. 3**, pink regions of interest, ROI). GLM coefficients in late cue/early delay ROIs were significantly negative, showing that power was suppressed by EV in each monkey in the dlPFC (Wilcoxon rank sum relative to 0: monkey 1: $p < 5\times10^{-28}$, monkey 2: $p < 2\times10^{-12}$) and in 7A (monkey 1: $p < 2\times10^{-21}$, monkey 2: $p < 9\times10^{-13}$). The same ROIs showed significant modulations by uncertainty in dlPFC (monkey 1: $p < 6\times10^{-10}$, monkey 2: $p < 8\times10^{-8}$) and in 7A (monkey 1: $p < 6\times10^{-6}$, monkey 2: $p < 2\times10^{-14}$). Consistent with the interaction in the monkeys' licking behavior, this ROI also showed a significant uncertainty x EV interaction, whereby EV produced a larger decrease in power (more negative coefficients) at increasing levels of uncertainty (**Fig. 3**, last column (2-way ANOVA; dlPFC: monkey 1: $p < 3\times10^{-49}$, monkey 2: $p < 4\times10^{-51}$; 7A; monkey 1: $p < 2\times10^{-21}$, monkey 2: $p < 5\times10^{-26}$). Given the common observation that α-band oscillations are

suppressed by attention and arousal[31], these findings most likely reflect higher arousal produced by uncertainty and EV.

In contrast with these uniform effects in the low frequency band, uncertainty and EV differentially affected the two areas in the high-β/low-γ frequency range (**Fig. 3**, purple traces). In the dlPFC, power in this band was suppressed by EV (late-cue ROI: monkey 1: $p < 4\times10^{-28}$, monkey 2: $p < 9.5\times10^{-4}$) and was enhanced by uncertainty (cue and delay ROI: monkey 1: $p < 3\times10^{-6}$, monkey 2: $p < 2\times10^{-22}$). Area 7A showed the opposite patterns, with late cue/early delay power increasing increase as a function of EV (**Fig. 3**, bottom row; monkey 1: $p < 2\times10^{-16}$, monkey 2: $p < 4\times10^{-18}$) and decreasing as a function of uncertainty (monkey 1: $p < 2\times10^{-13}$, monkey 2: $p < 4\times10^{-17}$). Both areas showed significant interactions whereby the effects of EV were intensified at higher levels of uncertainty (**Fig. 3**, right column). Higher uncertainty produced a stronger EV-induced suppression in power in the dlPFC (uncertainty×EV interaction: monkey 1: $p < 5\times10^{-8}$, monkey 2: $p < 10^{-30}$) and a stronger EV-induced increase in power in area 7A (monkey 1: $p < 2\times10^{-45}$, monkey 2: $p < 9\times10^{-16}$).

In sum, uncertainty and EV reduced power in the high-α/low-β frequency range in both areas, but had distinct area specific effects in the high-β/low-γ frequency range.

Uncertainty and EV have distinct single-neuron representations

To examine how uncertainty and EV are represented by individual cells, we fitted each neuron's firing rate during the cue and delay periods with the same GLM model we used for oscillatory power, which included EV, uncertainty, the EV x uncertainty interaction, and cue location as a nuisance regressor. This showed that EV and uncertainty were encoded in both 7A and dlPFC and, in each area, the two variables had clearly segregated neural representations (**Fig. 4** and **Table 1)**.

Over 24% of cells in each area showed significant sensitivity to uncertainty, EV or their interaction (**Table 1**, bottom row). In each area, the sensitive cells were equally likely to show positive or negative scaling – i.e., increases or decreases in firing as a function of uncertainty or EV (**Fig. 4A,B, Table 1**). Firing rate modulations were sustained, with their peaks centered broadly on the late cue/early delay epochs (**Fig. 4C**). Area 7A differed slightly from the dlPFC in that it showed stronger interaction effects (**Fig. 4A** vs **B** red points, and **Table 1**) and, across the entire population of cells, had a bias toward positive coding of EV (**Fig. 4B,** abscissa**;** the average signed EV coefficients in 7A were 0.171 ± 0.032, $p = 10^{-6}$ relative to 0; the other distributions showed no bias for positive or negative encoding of uncertainty or EV, all $p > 0.23$). Except for these minor differences, however, dlPFC and 7A showed equivalent prevalence and strength of uncertainty and EV modulations (**Table 1**).

A striking aspect of the activity in both areas is that the encoding of uncertainty and EV were strongly segregated. The GLM coefficients of the two factors were uncorrelated (Spearman r; dlPFC: 0.06, $p = 0.15$; $n = 530$; 7A: 0.03, $p = 0.49$; $n = 522$) and hardly any neurons had main effects of both factors. Confirming this segregation, cells with positive or negative encoding of uncertainty or EV had no corresponding trend for the other factor (**Fig. 4D**).

Given this stark segregation, we computed noise correlations - correlated fluctuations in trial by trial responses that are indicative of shared connectivity[32] – in order to examine whether neurons with different encoding profiles have distinct connectivity. We restricted this analysis to pairs of simultaneously recorded cells that had at least 10 trials in common for each task

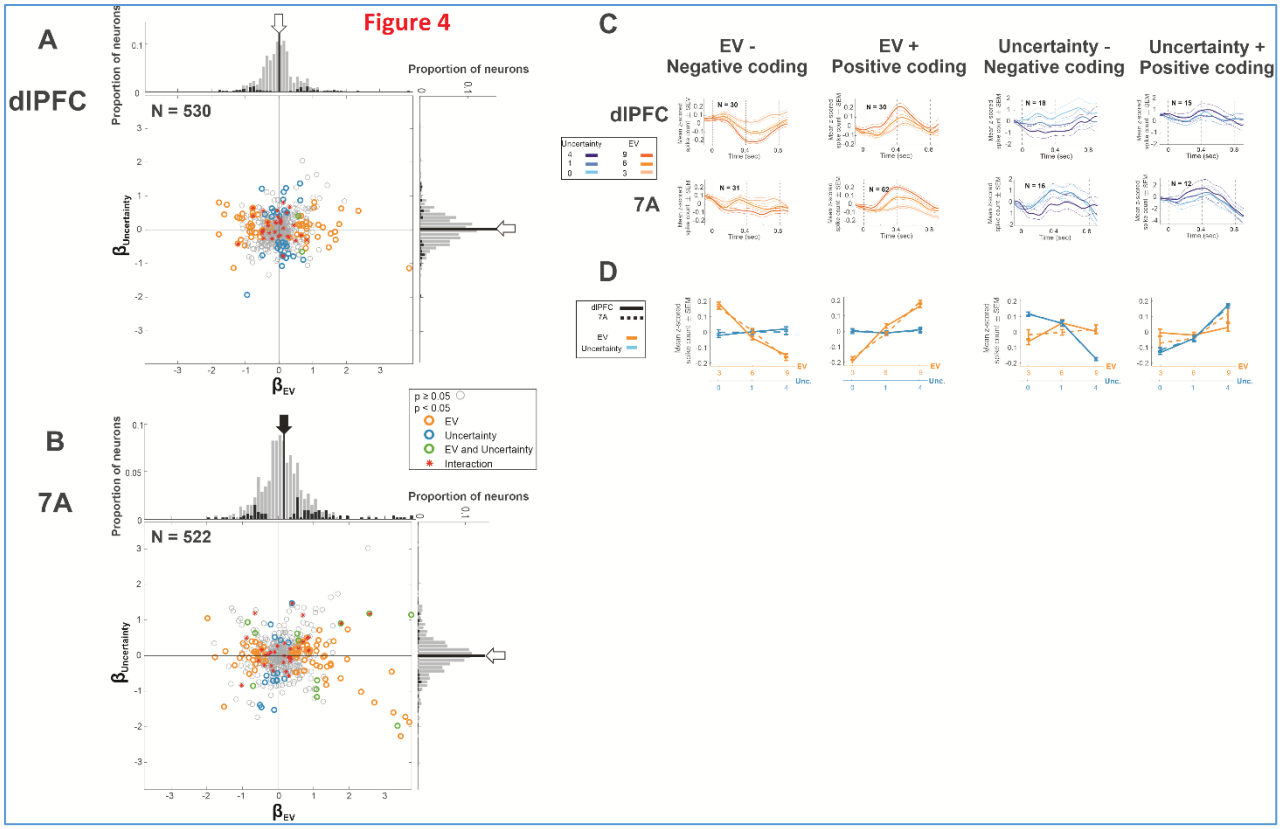

Fig. 4 Encoding of EV and uncertainty in single-neuron spiking activity (A,B) Comparisons of GLM coefficients measuring the effect of EV (β_{EV}, abscissa) and uncertainty ($\beta_{Uncertainty}$, ordinate) in individual neurons in the dlPFC (**A**) and 7A (**B**). Every point is one neuron, and the colors indicate cells with significant coefficients for uncertainty (blue), EV (orange) and interaction (red). Cells with significant main effects of both uncertainty and EV are shown in green. The marginal distributions show the significant coefficients in black, with the median indicated by a vertical line and arrow (black if the median is significantly different from 0, $p < 0.05$, Wilcoxon signed-rank test, and white otherwise). **(C) Peri-stimulus time histograms** for the subsets of cells with significant positive or negative coefficients of EV and uncertainty (including the few cells with both main effects). The traces show average z-scored spike counts aligned on cue onset, smoothed with a Gaussian kernel with 50 ms standard deviation, and sorted by EV (left two panels) and uncertainty (right two panels). **(D) Spike counts** of the subsets of cells shown in C as a function of EV (orange) and uncertainty (blue), for dlPFC (solid) and 7A (dashed). Each point shows the mean and SEM of the spike count in the interval of 0-800 ms after cue onset, z-scored within each cell and averaged across cells (error bars show SEM across cells).

condition. Importantly, we used firing rates in a 600 ms fixation epoch preceding the presentation of the reward cue, allowing us to estimate the shared connectivity between subsets of cells independently of their responses to uncertainty or EV.

Pairs of neurons in which both cells encoded EV, or both encoded uncertainty with similar polarity (i.e., both with positive or both with negative scaling) showed significant positive correlations in both areas (**Fig. 5**, "Within category, same polarity; dlPFC: $r = 0.29 \pm 0.04$, $p = 3.6\times10^{-7}$ relative to 0; 7A $r = 0.28 \pm 0.03$, $p = 2.1\times10^{-10}$ relative to 0; see **Table 2** for breakdown by response polarity). In contrast, coefficients were much smaller in pairs in which the two neurons had opposite polarity (Kruskal Wallis analysis of variance for same vs opposite polarity; dlPFC: EV: $p = 2\times10^{-5}$ ($n_{\text{same polarity}} = 33$, $n_{\text{opposite polarity}} = 21$ pairs); uncertainty: $p = 0.01$ ($n_{\text{same polarity}}$

= 14, $n_{opposite\ polarity}$ = 4 pairs); 7A: EV: $p = 2.6\times10^{-6}$ ($n_{same\ polarity}$ = 76, $n_{opposite\ polarity}$ = 61 pairs); uncertainty: p = 0.08; $n_{same\ polarity}$ = 3, $n_{opposite\ polarity}$ = 2 pairs).

Importantly, correlated variability, was also much weaker in "across-category" pairs where one neuron encoded uncertainty and the other EV (**Fig. 5**; Kruskal-Wallis test, within-category same polarity vs across-category pairs; dlPFC, n = 47 and n = 56, $p = 2.5\times10^{-7}$, n = 79 and n = 43, 7A $p = 5.1\times10^{-8}$), and this imbalance remained evident when the comparison was broken down by encoding polarity (**Table 2**). Thus, neurons that are sensitive to uncertainty or EV share connectivity as a function of their response polarity, but neurons sensitive to different variables have little shared connectivity.

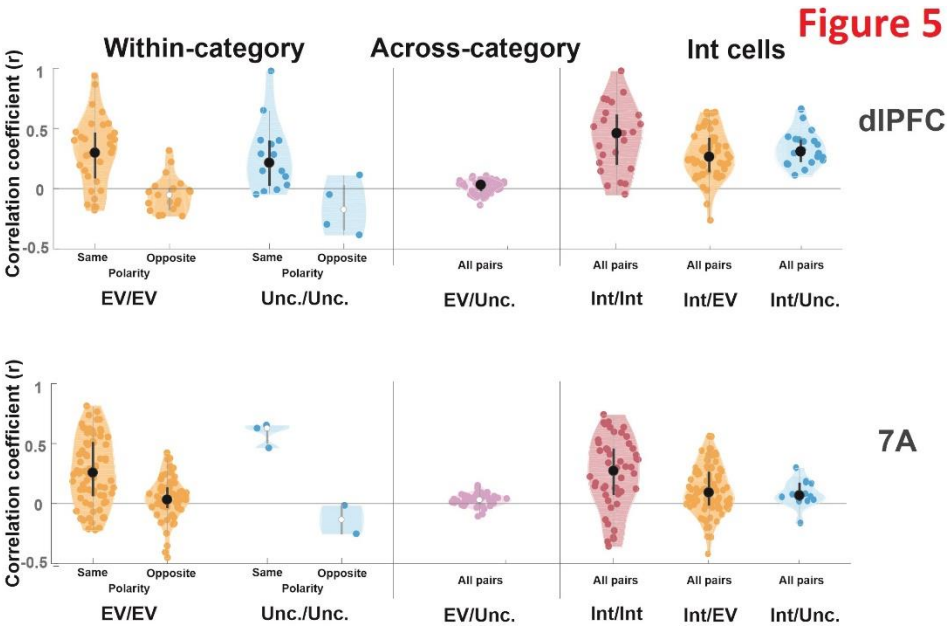

Fig. 5 Noise correlations Each violin plot shows the distributions of correlation coefficients between the trial-by-trial spike counts of simultaneously recorded pairs of cells. The dots in each plot show the median coefficient and the whiskers indicate the 25th and 75th percentiles. Black symbols show distributions that were significantly higher than 0 ($p < 0.05$). The cell pairs are separated according to their selectivity. The leftmost distributions show pairs in which both cells were selective to EV or both were selective for uncertainty, and the two cells had the same encoding polarity (EV+/EV+. EV-/EV-, uncertainty+/uncertainty+ or uncertainty-/uncertainty-) or opposite polarity (EV+/EV-. uncertainty+/uncertainty-). The middle column shows the coefficients for pairs in which one cell was selective for EV and the other for uncertainty (pooled across the sign or sign congruence of encoding). The right column shows the coefficients for pairs in which one cell showed an interaction and the other showed either an interaction (purple) or a main effect of EV (orange) or uncertainty (blue).

Pairs of neurons that showed only interactions between uncertainty and EV had positive noise correlations comparable to those for within-category same-polarity cells (**Fig. 5**, and **Table 2**, "Int cells"). Interestingly, however, the correlations between these neurons and those coding uncertainty and EV were significantly stronger than the across-category correlations between uncertainty and EV coding cells (Kruskal Wallis, dlPFC $p = 1.4\times10^{-5}$, 7A $p = 5.1\times10^{-4}$). Thus, neurons showing interactions may bridge between EV-coding and uncertainty-coding subnetworks.

In addition to the neurons with linear effects of uncertainty or EV, many more cells showed irregular, non-linear modulations. To estimate the total coding capacity, we used support vector machine (SVM) analysis to measure the decoding accuracy of the three levels of uncertainty and EV based on the firing rates in the entire neural population. Decoders that were trained and tested on the same variable achieved clearly above-chance pairwise classification in both 7A and dlPFC (**Fig. 6A**). However, decoders that were trained and tested in incongruent regimes

(i.e., training on uncertainty and testing on EV and vice-versa) performed only at chance (**Fig. 6B**) showing that the representations of uncertainty and EV are strongly segregated across the entire population of cells.

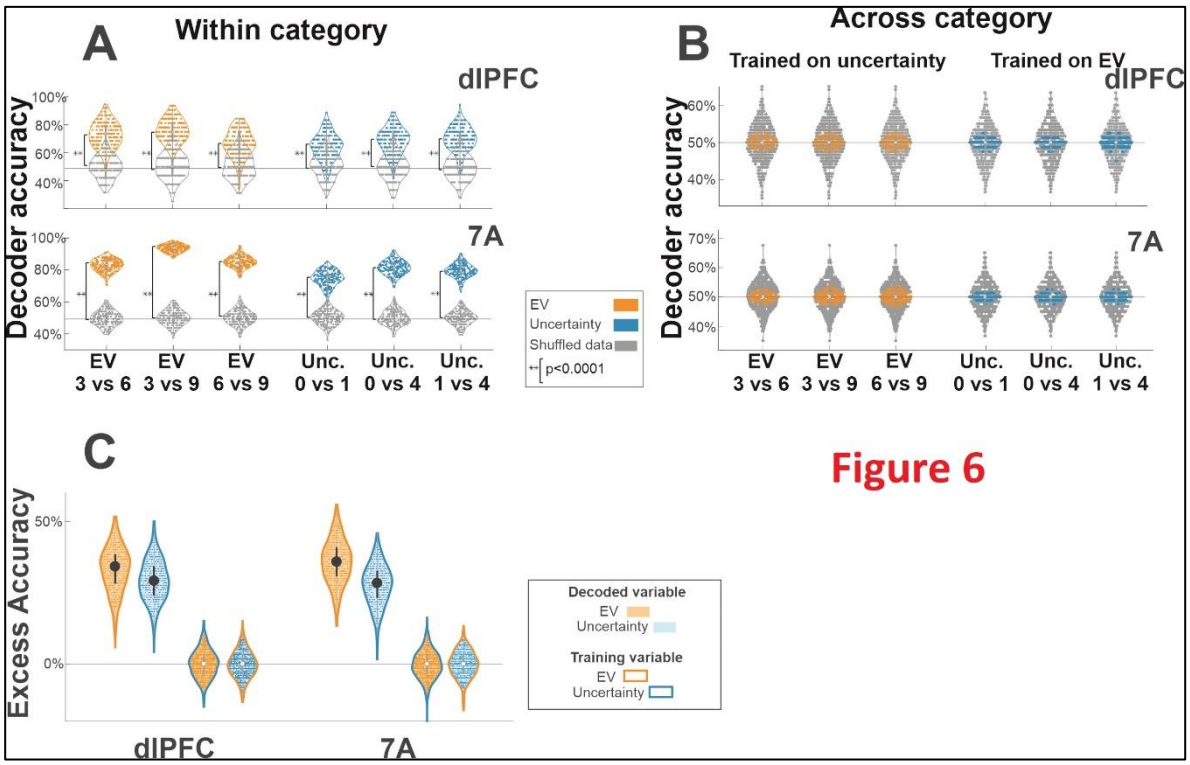

Fig. 6 Population decoding (A) Decoding accuracy for classifiers trained and tested on the same variable. Each violin plot shows the distribution of accuracy scores for binary classification of EV (orange) or uncertainty levels (blue) over 200 bootstrap iterations from the original dataset. Gray distributions show decoding accuracy for the same dataset with randomized labels. The dot and errorbars in each distribution show median and interquartile range. **(B) Decoding accuracy for classifiers trained and tested on the other variable.** All conventions as in **A**. **(C) Excess accuracy for all the conditions shown in A and B.** Each violin plot shows the distribution of the accuracy differences between the original and shuffled datasets across 200 bootstrap iterations, pooled across all the possible pairs of uncertainty or EV. The color of the dots indicates the variable that is decoded, and the color of the outline indicates the variable that was used for training. The dot and errorbars in each distribution show median and interquartile range. Darker colors indicate significant classification (excess accuracy greater than 0, $p < 0.05$).

Further analysis showed that decoding was stronger for EV than for uncertainty and was stronger in 7A relative to dlPFC. To document these results, we compared the distributions of excess accuracy (the differences in accuracy in the real and shuffled (null) data sets across 200 bootstrap interactions) using a 3-way ANOVA with train-test congruence, decoded variable (EV/uncertainty) and area as factors. We found a significant effect of congruence ($p = 0$), confirming that accuracy was much higher when the SVMs were trained and tested in congruent relative to incongruent regimes. For the congruent regime, decoding was better for EV than for uncertainty, as revealed by a significant variable*congruence interaction ($p = 1.1\times10^{-112}$), and by post-hoc tests showing that this difference held for both areas (Wilcoxon signed-rank test, congruent train-test regime, EV vs uncertainty: dlPFC: $p = 1.6\times10^{-17}$, 7A: $p = 1.8\times10^{-61}$). Finally, for the congruent regimes, decoding was better in 7A relative to the dlPFC, as shown by a significant area*congruence interaction ($p = 0.0032$), and post-hoc tests for uncertainty and EV

(Wilcoxon signed-rank test, congruent train-test regime, dlPFC vs 7A: EV: $p = 3.2\times10^{-11}$, uncertainty: $p = 4.0\times10^{-4}$).

Uncertainty enhances parietal to frontal information transmission

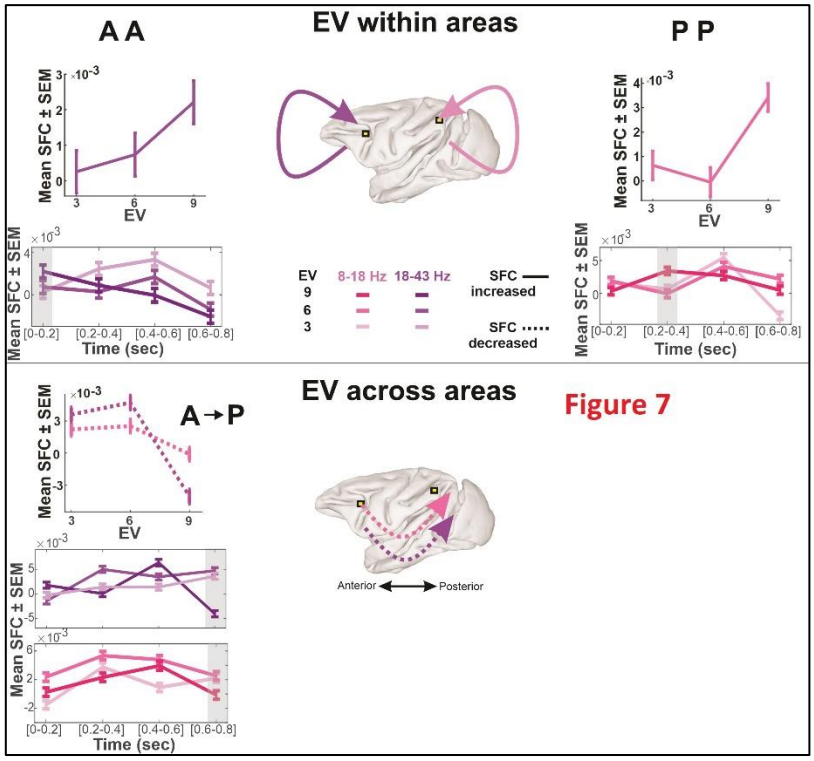

Fig. 7 The effects of EV on spike-field coherence (SFC) The arrows in the central cartoons summarize the effects of EV on SFC within each area (top) and between areas (bottom). Only effects that are statistically significant are shown, color coded by the frequency band, and by whether the change was an increase (solid) or decrease (dashed) in SFC as a function of EV. The columns flanking the cartoons provide details about the arrows in the cartoon. The top panels show the mean and SEM of the SFC values across all neuron-LFP channel pairs and all task conditions with identical level of EV. The plots underneath show the mean and SEM of the SFC values in 200 ms time intervals aligned to cue onset, and shading indicates intervals where the values were significantly sensitive to EV (Kruskal-Wallis test, $p < 0.034$).

The analysis of neural activity suggests that dlPFC and 7A have similar responses to reward and uncertainty, consistent with these areas' similar responses in other task contexts[33, 34]. We wondered, however, whether the exchange of information across the areas may be differentially influenced by uncertainty or EV. To examine this possibility, we focused on spike field coherence (SFC) – a measure of the degree to which spikes are emitted at a consistent phase of an LFP oscillation cycle[35-37] (see also *Methods*). SFC is particularly informative because it measures directional interactions. An increase in coherence between spikes recorded on electrode A and LFP oscillations on electrode B suggests that information transmission increases from A to B and not in the opposite direction.

Analysis of the SFC revealed that EV primarily enhanced SFC within each area, while uncertainty primarily affected information transmission across areas.

The primary effect of EV was an increase in SFC within both dlPFC and 7A (**Fig. 7**, top). These effects appeared during the cue period and consisted of an early increase within the dlPFC in the high-β/low-γ frequency band (mean±SEM EV_3: 0.00025±0.00059, EV_9: 0.0022±0.00060, n = 164880, Kruskal-Wallis test, $p = 0.03$), and a slightly later increase in 7A in the high-α/low-β frequency band (mean±SEM EV_3: 0.00064±0.00058, EV_9: 0.00341±0.00056, n = 136368, Kruskal-Wallis test, $p = 2.3\times10^{-17}$). In contrast, EV affected the across-areas transmission only at the end of the delay period, reducing SFC from dlPFC to 7A in both frequency bands (high-α/low-β: mean±SEM EV_3: 0.0022±0.0006, EV_9: -0.0001±0.0006, n = 164880, Kruskal-Wallis

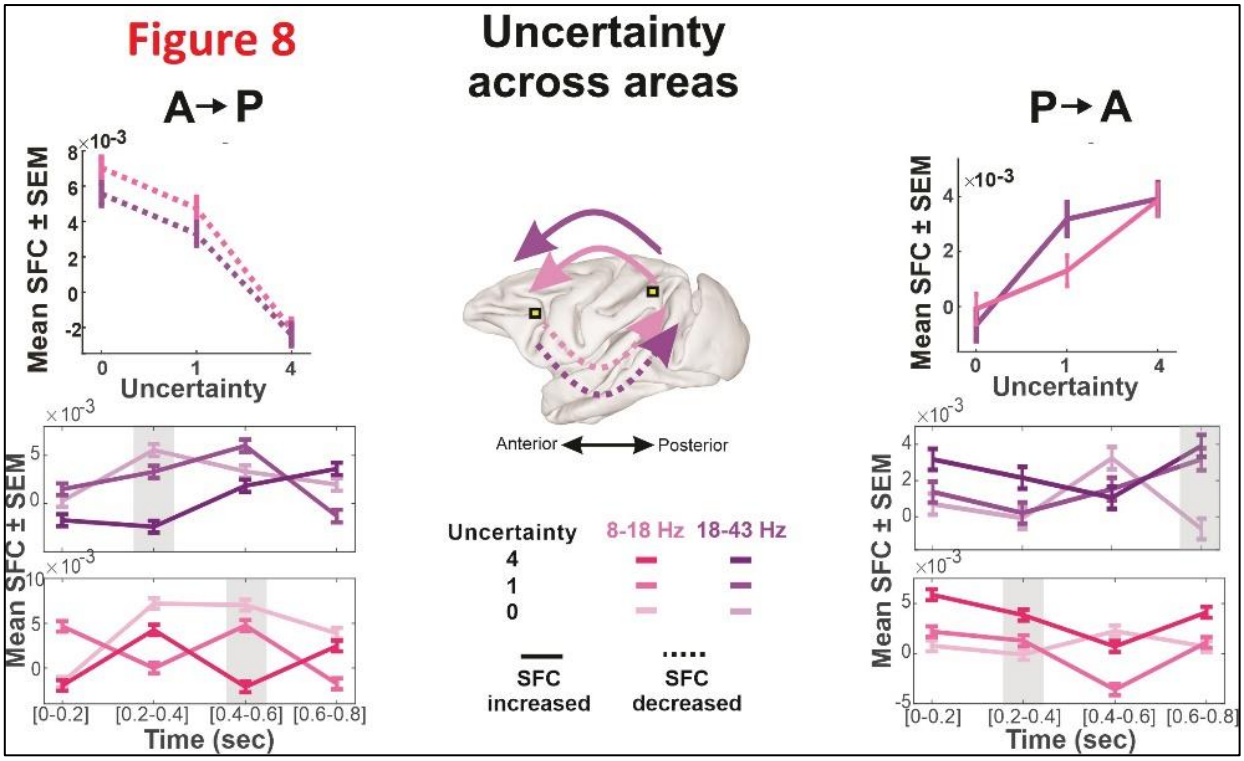

Fig. 8 The effects of uncertainty on spike-field coherence (SFC) across areas All conventions as in **Fig. 7**.

test, $p = 7.8\times10^{-12}$; high-β/low-γ: EV_3: 0.0036±0.0006, EV_9: -0.0041±0.0006, $p = 5.9\times10^{-30}$) with no change in the SFC from 7A to the dlPFC (**Fig. 7,** bottom).

In contrast, uncertainty had inconsistent effects within areas but primarily modulated SFC *between* areas. The across-area modulations were directional, consisting in a reduction in the SFC from dlPFC to 7A and enhancement of the transmission from 7A to the dlPFC (**Fig. 8**). These inter-area modulations were significant in both frequency bands and showed overlapping time courses. SFC from dlPFC to 7A showed an early suppression by uncertainty in the high-β/low-γ frequency band (mean±SEM var_0: 0.0055±0.0006, var_4: -0.0024±0.0006, Kruskal-Wallis test, $p = 1.8\times10^{-21}$), and a later suppression in the high-α/low-β frequency band (mean±SEM var_0: 0.0070±0.0006, var_4: -0.0021±0.0006, $p = 6.3\times10^{-16}$). SFC from 7A to dlPFC was significantly enhanced by uncertainty primarily in the high-α/low-β frequency band in the cue period (mean±SEM var_0: -0.00009±0.00054, var_4: 0.0038±0.0005, test, $p = 5.2\times10^{-8}$), and, to a lesser extent, in the high-β/low-γ frequency band in the late delay period (mean±SEM var_0: -0.0007±0.0006, var_4: 0.0093±0.0006,, $p = 3.5\times10^{-7}$). These changes could not be explained by modulations of LFP power, which affected the two bands in opposite directions in the two areas (cf **Fig. 3**), and could not be explained by LFP-LFP coherence, which showed only moderate increases with risk specific to the higher frequency band (**Fig. S2**), suggesting that they specifically indicate altered communication between frontal and parietal areas in response to reward uncertainty.

Discussion

We show that reward value and uncertainty exert common and divergent effects on areas 7A and the dlPFC. The main modulation that was common to reward and uncertainty was a reduction in LFP power in the high α/low-β frequency bands, which was prominent in both 7A and the dlPFC. Since decreases in alpha oscillations are associated with enhanced task engagement and task-related attention in humans and monkeys[31], this finding suggests that the effects we observed encoded arousal produced by higher uncertainty and higher EV. Beyond this common effect, uncertainty and EV produced several divergent modulations of spiking activity, LFP and neural communications, suggesting that the two variables are associated with distinct patterns of fronto-parietal activity.

Perhaps the clearest dissociation revealed by our data was in the individual neuron spiking activity. In both 7A and dlPFC, subsets of neurons encoded either uncertainty or EV but almost never both quantities. Moreover, although each quantity was readily decoded from population activity, cross-decoding attempts failed. Finally, analysis of noise correlations suggests that, although cells encoding uncertainty or EV formed subnetworks with shared connectivity (subject to encoding polarity) there was little shared connectivity among neurons coding uncertainty and those coding EV. Together, these findings support the conclusion that the brain explicitly signals uncertainty as a *bona-fide* quantity rather than merely a secondary aspect of reward distributions. This conclusion is consistent with previous findings in subcortical structures and the orbitofrontal cortex[27-29], and our results show that it extends to the fronto-parietal network involved in cognitive regulation.

We recently proposed that an explicit representation of uncertainty is critical for the efficient focusing on attention and cognitive effort on situations that are not only associated with consequential outcomes but, importantly, benefit from new information (i.e., a further reduction of uncertainty) [25, 38] (see[39] for a related view). In support of this view, saccades made with the prospect of obtaining new information are associated with more attentional effort and higher pre-saccadic activity in area LIP relative to rewarded saccades that merely confirm prior expectations[40]. Moreover, LIP neurons[40], like those in the OFC[41], encode expected gains in information independently of expected gains in reward, even in tasks in which the two quantities are closely associated. An important direction for future research, therefore, is to further elucidate the pathways mediating the recruitment of attention and other cognitive actions for reducing uncertainty about utility-relevant outcomes.

A second set of dissociations that emerged from our data is between the effects of uncertainty and EV in higher-frequency LFP oscillations and SFC connectivity. Most importantly, while EV enhanced SFC within 7A and the dlPFC, uncertainty primary modulated *across-area* connectivity. Higher uncertainty was associated with reduced transmission from the frontal to the parietal lobe but enhanced transmission in the opposite direction, from 7A to the dlPFC.

These results extend current hypotheses about the neural effects of uncertainty, which emerge from *in vitro* recordings and behavioral manipulations in rats but have not been extensively tested in non-human primates. These hypotheses propose that uncertainty is signaled by neuromodulators including dopamine, acetylcholine (ACH) and norepinephrine (NE)[2, 42], and that it is associated with lower top-down connectivity and enhanced transmission of bottom-up information[42]. A parallel hypothesis is that the parietal cortex plays a special role in “attention for

learning" by enhancing the associability (attentional weight) of stimuli with uncertain reward history[43].

Our findings provide support for these views in the monkey fronto-parietal network, the primary animal model of attention control. The results are particularly consistent with the proposed importance of the parietal cortex in reasoning under uncertainty. While previous studies have shown that LIP neurons encode attentional orienting to novel stimuli[44], and respond robustly to salient stimuli that are inhibited in the dlPFC[13], our present results implicate 7A in responses to uncertainty independently of salience or novelty. Remarkably, our finding that 7A and dlPFC have similar uncertainty and reward-related spiking activity, suggest that a functional specialization may not be mediated by distinct neural activity but by distinct regimes of fronto-parietal connectivity.

Our finding that, in contrast with uncertainty, EV had weaker effects on within-area connectivity and only modestly reduced frontal to parietal SFC may seem counterintuitive given the presumed importance of top-down communication for maintaining memories of the task context and rules[17]. However, we propose that this finding is explained by our use of an instructed, rather than choice, paradigm. Parietal and premotor areas show enhanced SFC in low alpha/high beta frequency bands when animals make freely chosen rather than instructed actions[45], suggesting that the moderate reduction in SFC we observed was related to the monkeys' need to suppress inappropriate choice-related activity.

Our finding that higher EV primarily enhanced processing *within* dlPFC and 7A but not across areas, suggests that, while uncertainty promotes network-wide interactions, higher rewards may promote more segregated cortical function. This interpretation may explain the recent report that FEF saccade-related activity is more focused (stronger and shorter latency) during exploitative relative to exploratory epochs[46]. It may also explain the fact that, in a task in which monkeys focused on a target location while ignoring intervening distractors, distractor-related activity was prominent in LIP but was blocked from driving spiking in the dlPFC[13]. Thus, an important question for future research is the extent to which exploitative and exploratory contexts are associated with different configurations of fronto-parietal networks mediating attention regulation.

Methods

General methods. Data were collected from two adult male rhesus monkeys (Macaca mulatta; 9-12kg) using standard behavioral and neurophysiological techniques as described previously (Oristaglio et al. 2006). All methods were approved by the Animal Care and Use Committees of Columbia University and New York State Psychiatric Institute as complying with the guidelines within the Public Health Service Guide for the Care and Use of Laboratory Animals. Visual stimuli were presented on a MS3400V XGA high definition monitor (CTX International, INC., City of Industry, CA; 62.5by 46.5 cm viewing area). Eye position was recorded using an eye tracking system (Arrington Research, Scottsdale, AZ). Licking was recorded using an in-house device that detected interruptions in a laser beam produced by extensions of the monkeys' tongue to obtain water rewards.

Task A trial started with the presentation of two textured square placeholders (1 º width) located along the horizontal meridian at 8º eccentricity to the right and left of a central fixation point (white square, 0.2º diameter). After a 300-500 ms period of central fixation (when the monkeys maintained gaze within a 1.5-2º square window centered on the fixation point) one of the placeholders was replaced by a randomly selected reward cue (a vertical rectangle measuring 1.2 x 5º with 11 gray bars indicating the reward scale, and one or two gradations highlighted in yellow, indicating the trial's rewards). The cue remained visible for 400 ms and was followed by a 400ms delay period, after which the fixation point disappeared and one of the placeholders simultaneously increased in luminance, indicating the saccade target. The target location was randomized independently of the reward cue. If the monkey made a saccade to the target with a reaction time (RT) of 100 ms – 700 ms and maintained fixation within a 2.0-3.5º window of it for 377 ms, he received a reward with the magnitude and probability that had been indicated by the cue.

Neural recordings. After completing behavioral training, each monkey was implanted with two 50-electrode Utah arrays (electrode length 1.5 mm) arranged in rectangular grids (1 mm spacing; monkey 1, 7x7 mm, monkey 2, 5x10 mm) and positioned in the pre-arcuate portion of the dlPFC and the posterior portion of area 7A (**Figure S1**). Data were recorded using the Cereplex System (Blackrock, Salt Lake City, Utah) over 24 sessions spanning 4 months after array implantation in monkey 1, and 11 sessions spanning 2 months after implantation in monkey 2.

Data analysis We analyzed a total of 12,029 trials that (1) were correctly completed and (2) had RT within 2 standard deviations relative to the mean of each monkey's full data set (monkey 1: n = 8,082 analyzed trials, monkey 2: n = 3,947. Data were analyzed with MatLab (MathWorks, Natick, MA; version R2016-b) and other specialized software as noted below.

Licking The lickometer signal was digitized at 1 kHz using a 2.5 volt threshold, producing a trial by trial record of licking with 1 ms resolution. The probability of licking probability was measured in a 400 ms time window centered on the time of each monkey's average peak licking response (monkey 1: 400-800 ms after cue onset; monkey 2: 800-1,100 ms after cue onset). Licking probabilities in individual trials were normalized by subtracting the session's mean, pooled across sessions and subjected to a generalized linear model (GLM) analysis with EV, uncertainty, the EV×uncertainty interaction, and cue position and target position as nuisance regressors (using a binomial distribution and logit link function and implemented in the fitglm function in the MATLAB statistics toolbox). Models that included a parametric uncertainty

regressor outperformed those that included only a binary indicator of probabilistic versus deterministic cues, and are presented throughout the paper.

LFP pre-processing The raw local field potentials (LFP) from each electrode and trial were measured from 1,200 ms before to 2,000 ms after cue onset, notch filtered at 60Hz, low pass filtered at 100Hz and subjected to a linear trend removal. The traces from each session were then pooled and subjected to a two-step cleaning procedure to remove outliers in, respectively, the frequency and time domains. For the first step that removed outliers in the frequency domain, we calculated the power spectrum of each LFP trace in the range of 0 - 90 Hz (using a multi-taper method with 4 tapers) and characterized each trial with a 5-dimensional vector containing the sum of the logarithm of the power spectrum in 5 frequency bands (0.5-4 Hz, 4-8 Hz, 8-12 Hz, 12-30 Hz and 30-90 Hz). We then reduced the dimensionality of each session's data set to 2 principal components using principal component analysis, and clustered this 2-dimensional data set using Gaussian Mixture Models (GMM; *fitgmdist* function in the MATLAB *statistics and machine learning toolbox*). This procedure produced, for each session, one or two "dense" clusters that contained most of the session's data, and one or two "sparse" clusters containing the remaining trials, in which the LFP power in at least one frequency band was an outlier. We discarded the trials in the sparse clusters. In addition, we discared trials that were identified as outliers within the dense clusters - i.e., for which the Mahalanobis distance to all other trials in the cluster was above the 90% percentile. The trials surviving the first step were subjected to a second step that removed outliers in the time domain. To this end, we computed the peak-to-peak amplitude of the broadband LFP trace in each trial, z transformed these values, and removed trials for which this measure was more than half a standard deviation away from the mean across all trials. This was a conservative cleaning procedure that removed all the trials with poor signal quality due to a variety of reasons (e.g., signal to noise ratio, artefact or saturation). Overall, 39.5% of trials (12.3% to 77.4% across sessions) were excluded after preprocessing.

LFP power spectrum For each trial that was accepted for analysis, we calculated the LFP power spectrum in 1 Hz frequency bands using Morlet wavelet transformation (*ft_freqanalysis* function of the FieldTrip toolbox[47]. The power in each band was then z-scored relative to all the trials and time points within the session, and normalized relative to the trial's baseline using the following equation:

$$Relative\ Power\ Change(t,f) = \frac{Power_{tf} - \overline{baseline}_f}{\overline{baseline}_f} \qquad \text{eq. 1}$$

where $Power_{tf}$ is the power at time t and frequency f, and $\overline{baseline}_f$ is the power in frequency f during the 300 ms time interval before cue onset on the same trial. By normalizing relative to the frequency-specific baseline, this procedure accounts both for trial by trial variability and 1/f power distribution[37].

GLM of LFP power spectrum The *Relative Power Change* quantity from eq. 1 produced a time-frequency map of normalized LFP power for each trial and electrode. To determine how these maps varied as a function of uncertainty and EV, we pooled the trials across sessions and electrodes within each array, and fit this pooled dataset using a GLM with factors of [EV, uncertainty, EV×uncertainty, Cue location] assuming a normal distribution and identity link function. This produced a time-frequency map of coefficients measuring the effects of EV, uncertainty, and their interaction, controlling for any visuo-spatial response (**Fig. 3**). To identify regions of interest within the GLM coefficient maps, we divided the cue and delay periods into 200 ms epochs, and identified frequencies for which the coefficients for a variable were

significantly different from 0 with the same sign in both monkeys (Kruskal-Wallis test with False Discovery Rate (FDR) correction).

Single neurons spike analysis Raw spikes were sorted offline and produced a total of 1,175 neurons in dlPFC (749 in monkey 1) and 971 neurons in 7A (755 in monkey 1). We focused the analysis on the subset of units that were well isolated, had at least 5 trials in each condition, and fired at least 5 spikes on average within the time interval from 500 ms before to 1,000 ms after cue onset, comprising 530 neurons in dlPFC (432 in monkey 1) and 522 neurons in 7A (481 in monkey 1).

To measure neuronal selectivity, we fit each neuron's trial-by-trial spike count in the interval 0 – 800 ms after cue onset using a GLM with factors EV, uncertainty, EV×uncertainty, and Cue location, using a normal distribution and identity link function. To estimate changes in firing rate variability, we computed the Fano factor – the ratio of across-trial variability to the mean firing rate. Although the Fano factor was lower during the cue/delay relative to the pre-cue epochs, we found no consistent changes as a function of uncertainty or EV in either area.

SVM classification: We smoothed the raw spike train using a Gaussian kernel of 50 ms standard deviation, and measured the average smoothed firing rate in each trial in the interval 0 – 800 ms after cue onset. We then evaluated decoding accuracy for each pairwise classification (e.g., EV3 vs EV6, uncertainty 1 vs uncertainty 4, etc) using the data pooled across all the neurons in an array. To construct the pooled dataset, we randomly selected *m* trials from each neuron and every condition, where *m* was equal to the minimum number of trials, allowing each neuron to contribute to the analysis. We used a 5-fold cross-validation procedure with 200 repetitions to compute decoding accuracy in the original data set, and repeated the procedure after randomly shuffling trial labels to compute the baseline accuracy expected purely by chance.

Field-field coherence was measured using weighted phase lag index (WPLI)[36]. The WPLI uses imaginary part of the cross spectrum to remove the volume conduction effect. Within a session, for every task condition the phase locking index was calculated across trials and LFP channel pairs for every time and frequency. GLM with EV, uncertainty and EV×uncertainty factors was then fitted to the coherence maps from different sessions, assuming normal distribution and identity link function.

Spike-field coherence: We used the FieldTrip toolbox[47] to calculate the power spectrum for the trial-by-trial LFP using multitaper analysis, and the *ft_spiketriggeredspectrum* function to measure the phase in frequencies of 4-47 Hz. We estimated SFC using the average Pairwise Phase Consistency index (PPC2, *ft_spiketriggeredspectrum_stat* function), which is known to minimize biases due to low spike counts and volume conduction[35, 36]. For every pair of neuron-LFP channel, in each task condition and frequency, PPC2 was calculated across all spikes that the cell fired in the corresponding task condition. PPC2 values of all cell-LFP pairs (excluding pairs in which the neurons did not emit any spikes) were submitted to non-parametric analyses to detect influences of EV and uncertainty (n ranging between 136,368 and 164,880 across conditions).

Table 1 In the left column, the entries show the fraction (number) of neurons with significant coefficients for the respective variable in each area, and the results of chi-square tests of proportions across areas. In the right column, the entries show the mean ± SEM of the coefficients in the sensitive cells. The "All EV sensitive", "All unc. sensitive" and "All interaction" entries give the mean ± SEM of the signed coefficients in each category. However, the rightmost column gives the result of a Kruskall-Wallis test between the absolute values of the coefficients, indicating the extent to which effects are stronger in a specific area.

	Proportion significant			**β values (mean ± SEM)**		
	dlPFC	**7A**	**dlPFC vs 7A**	**dlPFC**	**7A**	**dlPFC vs 7A**
EV						
EV+	5.7% (30)	12% (62)	$\chi2$ = 2.410, df =1, p > 0.1	1.13 ± 0.13*	1.32 ± 0.11*	p = 0.72
EV-	5.7% (30)	6% (31)	$\chi2$ = 0.007, df =1, p > 0.9	-0.94 ± 0.07*	-0.80 ± 0.07*	p = 0.06
All EV sensitive	11.3% (60)	18% (93)	$\chi2$ = 1.690, df =1, p > 0.1	0.10 ± 0.15	0.61 ± 0.13*	p = 0.70
Uncertainty						
Unc.+	2.8% (15)	2.3% (12)	$\chi2$ = 0.060, df =1, p > 0.1	0.73 ± 0.09*	0.79 ± 0.1*	p = 0.62
Unc.-	3.4% (18)	3.1% (16)	$\chi2$ = 0.017, df =1, p > 0.9	-0.72 ± 0.08*	-0.95 ± 0.1*	p = 0.10
All unc. sensitive	6.2% (33)	5.4% (28)	$\chi2$ = 0.070, df =1, p > 0.1	-0.06 ± 0.14	-0.20 ± 0.18	p = 0.08
Interaction						
All interaction	6.6% (35)	6.1% (32)	$\chi2$ = 0.018, df =1, p > 0.9	0.04 ± 0.18	0.82 ± 0.23*	p = 0.04
All modulations	22% (117)	26% (134)	$\chi2$ = 3.460, df = 7, p > 0.1			

Table 2 Each entry shows the average and SEM of the Pearson correlation coefficient, and the number (N) of simultaneously recorded cell pairs of each type that met the analysis criteria (see *Methods*). Stars and bold typeface indicate the results of signed-rank tests relative to 0: ****p < 0.01**; *p < 0.05

When all pairs are considered, coefficients did not differ in dlPFC relative to 7A (Kruskal-Wallis test, p > 0.1)

	dlPFC					**7A**				
	EV+	EV-	Unc.+	Unc.-	Int.	EV+	EV-	Unc.+	Unc.-	Int.
EV+	**0.34±0.06**** **N = 23**	-0.05±0.03 N = 21	0.00±0.02 N = 9	**0.04±0.01**** **N = 25**	**0.18±0.04**** **N = 28**	**0.26±0.04**** **N = 59**	0.04±0.02* N = 61	0.06±0.02* N = 6	-0.00±0.01 N = 18	**0.14±0.03**** **N = 55**
EV-		0.20±0.06* N = 10	-0.02±0.02 N = 10	-0.00±0.01 N = 12	0.08±0.05 N = 26		**0.29±0.07**** **N = 17**	0.02±0.02 N = 4	0.00±0.01 N = 15	0.06±0.03 N = 33
Unc. +			1.14±0.08 N = 6	-0.16±0.11 N = 4	0.2±0.05* N = 7			N.A. N = 0	-0.14±0.12 N = 2	0.01±0 N = 1
Unc.-				0.36±0.11* N = 8	**0.19±0.05**** **N = 13**				0.58±0.06 N = 3	0.09±0.04* N = 11
Int					**0.30±0.07**** **N = 25**					**0.24±0.04**** **N = 50**

References

1. Schultz, W. Neuronal Reward and Decision Signals: From Theories to Data. *Physiol Rev.* **95**, 853-951 (2015).
2. Bach, D.R. & Dolan, R.J. Knowing how much you don't know: a neural organization of uncertainty estimates. *Nat Rev Neurosci* **13**, 572-586 (2012).
3. Braver, T.S. *et al.* Mechanisms of motivation-cognition interaction: challenges and opportunities. *Cogn Affect Behav Neurosci* **14**, 443-472 (2014).
4. Gershman, S.J., Horvitz, E.J. & Tenenbaum, J.B. Computational rationality: A converging paradigm for intelligence in brains, minds and machines. *Science* **349**, 273-278 (2015).
5. Shenhav, A., Botvinick, M. & Cohen, J. The expected value of control: an integrative theory of anterior cingulate cortex function. *Neuron* **79**, 217-240 (2013).
6. Padmala, S. & Pessoa, L. Reward reduces conflict by enhancing attentional control and biasing visual cortical processing. *J Cogn Neurosci* **23**, 3419-3432 (2011).
7. Engelmann, J.B., Damaraju, E., Padmala, S. & Pessoa, L. Combined effects of attention and motivation on visual task performance: transient and sustained motivational effects. *Front Hum Neurosci* **3**, 4 (2009).
8. Green, J.J. *et al.* Cortical and Subcortical Coordination of Visual Spatial Attention Revealed by Simultaneous EEG-fMRI Recording. *J Neurosci* **37**, 7803-7810 (2017).
9. Krebs, R.M., Boehler, C.N., Egner, T. & Woldorff, M.G. The neural underpinnings of how reward associations can both guide and misguide attention. *J Neurosci* **31**, 9752-9759 (2011).
10. Cavada, C. & Goldman-Rakic, P.S. Posterior parietal cortex in rhesus monkey: II. Evidence for segregated corticocortical networks linking sensory and limbic areas with the frontal lobe. *J. Comp. Neurol.* **287**, 422-445 (1989).
11. Saleem, K.S., Miller, B. & Price, J.L. Subdivisions and connectional networks of the lateral prefrontal cortex in the macaque monkey. *J Comp Neurol.* **522**, 1641-1690 (2014).
12. Katsuki, F. & Constantinidis, C. Unique and shared roles of the posterior parietal and dorsolateral prefrontal cortex in cognitive functions. *Front Integr Neurosci* **6**, 17 (2012).
13. Suzuki, M. & Gottlieb, J. Distinct neural mechanisms of distractor suppression in the frontal and parietal lobe. *Nature Neuroscience* **16**, 98-104 (2013).
14. Bisley, J.W. & Goldberg, M.E. Attention, intention, and priority in the parietal lobe. *Annual Review of Neuroscience* **33**, 1-21 (2010).
15. Thompson, K.G. & Bichot, N.P. A visual salience map in the primate frontal eye field. *Prog Brain Res* **147**, 251-262 (2005).
16. Stoet, G. & Snyder, L.H. Single neurons in posterior parietal cortex of monkeys encode cognitive set. *Neuron* **42**, 1003-1012 (2004).
17. Crowe, D.A. *et al.* Prefrontal neurons transmit signals to parietal neurons that reflect executive control of cognition. *Nat Neurosci* **16**, 1484-1491 (2013).
18. Kennerley, S.W. & Wallis, J.D. Reward-dependent modulation of working memory in lateral prefrontal cortex. *J Neurosci* **29**, 3259-3270 (2009).
19. Asaad, W.F., Lauro, P.N., Perge, J.A. & Eskandar, E.N. Prefrontal Neurons Encode a Solution to the Credit-Assignment Problem. *J Neurosci.* **37**, 6995-7007 (2017).
20. Asaad, W.F. & Eskandar, E.N. Encoding of both positive and negative reward prediction errors by neurons of the primate lateral prefrontal cortex and caudate nucleus. *J Neurosci.* **31**, 17772-17787 (2011).

21. Mansouri, F.A., Egner, T. & Buckley, M.J. Monitoring Demands for Executive Control: Shared Functions between Human and Nonhuman Primates. *Trends Neurosci* **40**, 15-27 (2017).
22. Schultz, W. Neuronal Reward and Decision Signals: From Theories to Data. *Physiol Rev* **95**, 853-951 (2015).
23. McGuire, J.T., Nassar, M.R., Gold, J.I. & Kable, J.W. Functionally dissociable influences on learning rate in a dynamic environment. *Neuron* **84**, 870-881 (2014).
24. Daddaoua, N., Lopes, M. & Gottlieb, J. Intrinsically motivated oculomotor exploration guided by uncertainty reduction and conditioned reinforcement in non-human primates. *Sci Rep* **6** (2016).
25. Gottlieb, J. & Oudeyer, P.Y. Toward a neuroscience of active sampling and curiosity. *Nat Rev Neurosci.* **19**, 758-770 (2018).
26. Schultz, W. *et al.* Explicit neural signals reflecting reward uncertainty. *Philos Trans R Soc Lond B Biol Sci* **363**, 3801-3811 (2008).
27. O'Neill, M. & Schultz, W. Coding of reward risk by orbitofrontal neurons is mostly distinct from coding of reward value. *Neuron* **68**, 789-800 (2010).
28. Monosov, I.E. & Hikosaka, O. Selective and graded coding of reward uncertainty by neurons in the primate anterodorsal septal region. *Nat Neurosci* **16**, 756-762 (2013).
29. Monosov, I.E., Leopold, D.A. & Hikosaka, O. Neurons in the Primate Medial Basal Forebrain Signal Combined Information about Reward Uncertainty, Value, and Punishment Anticipation. *Journal of Neuroscience* **35**, 7443-7459 (2015).
30. Sullivan, B.T., Johnson, L., Rothkopf, C.A., Ballard, D. & Hayhoe, M. The role of uncertainty and reward on eye movements in a virtual driving task. *J. Vis.* **12** (2012).
31. Van Diepen, R.M., Foxe, J.J. & Mazaheri, A. The functional role of alpha-band activity in attentional processing: the current zeitgeist and future outlook. *Curr Opin Psychol* **29**, 229-238 (2019).
32. Cohen, M.R. & Kohn, A. Measuring and interpreting neuronal correlations. *Nat Neurosci* **14**, 811-819 (2011).
33. Chafee, M.V. & Goldman-Rakic, P.S. Matching patterns of activity in primate prefrontal area 8a and parietal area 7ip neurons during a spatial working memory task. *J. Neurophysiol.* **79**, 2919-2940 (1998).
34. Katsuki, F. & Constantinidis, C. Early involvement of prefrontal cortex in visual bottom-up attention. *Nat Neurosci* **15**, 1160-1166 (2012).
35. Vinck, M., Battaglia, F.P., Womelsdorf, T. & Pennartz, C. Improved measures of phase-coupling between spikes and the local field potential. . *J. Comput. Neurosci.* **33**, 53–75 (2012).
36. Martin Vinck, M., Oostenveld, R., van Wingerden, M., Battaglia, F. & Pennartz, C.M.A. An improved index of phase-synchronization for electrophysiological data in the presence of volume-conduction, noise and sample-size bias *NeuroImage* **55**, 1548–1565 (2011).
37. Cohen, M.X. *Analyzing neural time series data: theory and practice*. (MIT Press, 2014).
38. Gottlieb, J., Hayhoe, M., Hikosaka, O. & Rangel, A. Attention, reward and information seeking. *Journal of Neuroscience* **34**, 15497-154504 (2014).
39. Fan, J. An information theory account of cognitive control. *Front Hum Neurosci.* **8** (2014).
40. Horan, M., Daddaoua, N. & Gottlieb, J. Parietal neurons encode information sampling based on decision uncertainty. *Nat Neurosci* **22**, 1327-1335 (2019).
41. Blanchard, T.C., Hayden, B.Y. & Bromberg-Martin, E.S. Orbitofrontal cortex uses distinct codes for different choice attributes in decisions motivated by curiosity. *Neuron* **85**, 602-614 (2015).

42. Yu, A.J. & Dayan, P. Uncertainty, neuromodulation, and attention. *Neuron* **46**, 681-692 (2005).
43. Pearce, J.M. & Mackintosh, N.J. *Two theories of attention: a review and a possible integration*. (Oxford University Press, New York; 2010).
44. Foley, N.C., Jangraw, D.C., Peck, C. & Gottlieb, J. Novelty enhances visual salience independently of reward in the parietal lobe. *J neurosci* **34**, 7947-7957 (2014).
45. Pesaran, B., Nelson, M.J. & Andersen, R.A. Free choice activates a decision circuit between frontal and parietal cortex. *Nature* **453**, 406-409 (2008).
46. Ebitz, R.B., Albarran, E. & Moore, T. Exploration disrupts choice-predictive signals and alters dynamics in prefrontal cortex. *Neuron* **97**, 450-461 (2018).
47. Oostenveld, R., Fries, P., Maris, E. & Schoffelen, J.-M. FieldTrip: Open source software for advanced analysis of MEG, EEG, and invasive electrophysiological data. *Comput. Intell. Neurosci.* **156869** (2011).

Fig. S1

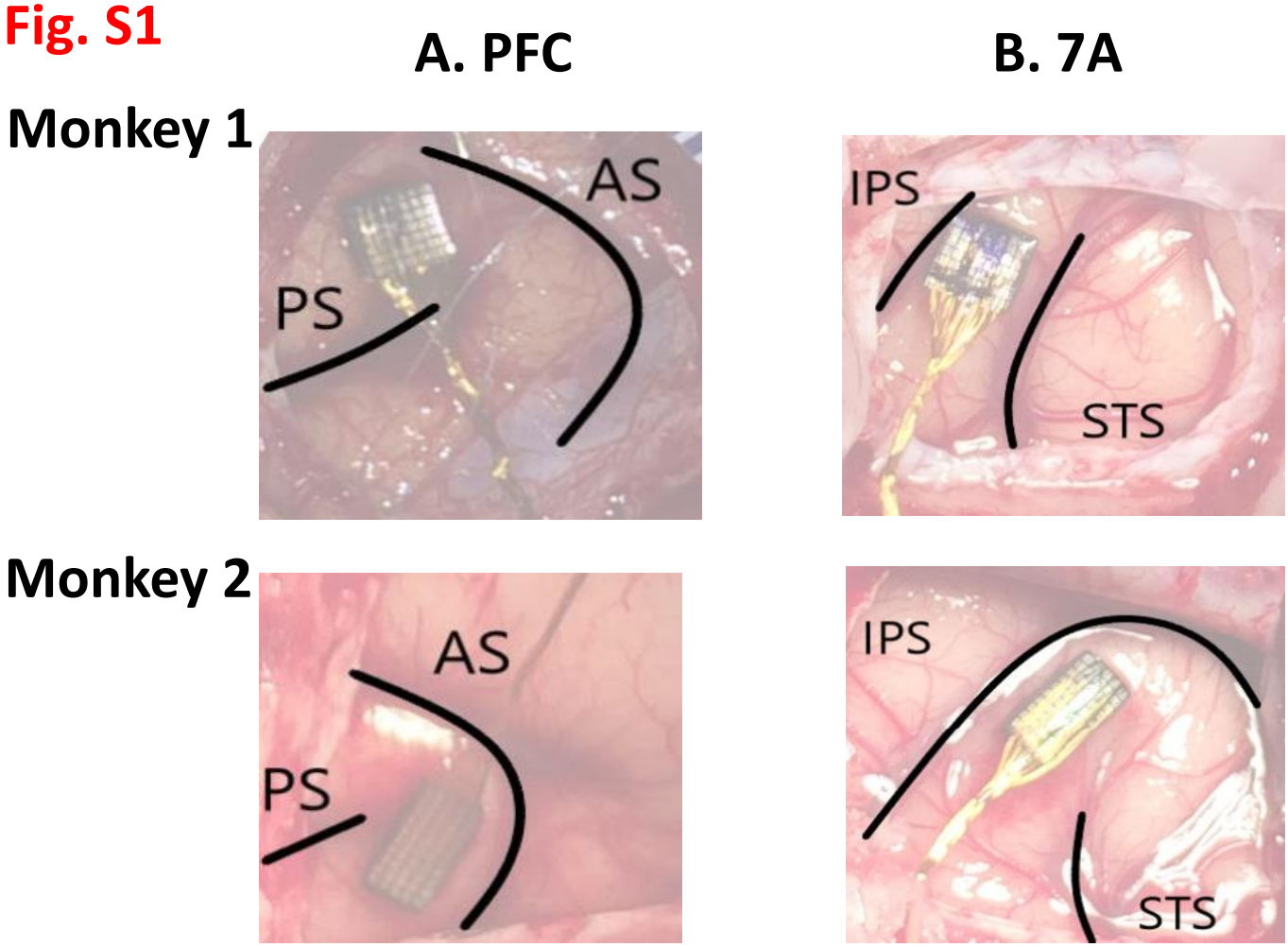

Figure S1. **Recording sites.** Intraoperative photographs showing array placements. (**A**) The dlPFC arrays were implanted between the arcuate sulcus (AS) and the principal sulcus (PS), slightly more dorsal in monkey 1 relative to monkey 2 because of vascular anatomy. (**B**) The 7A arrays were implanted between the intraparietal sulcus (IPS) and superior temporal sulcus (STS), in the posterior portion of this area that has been targeted in recent studies.

Fig. S2

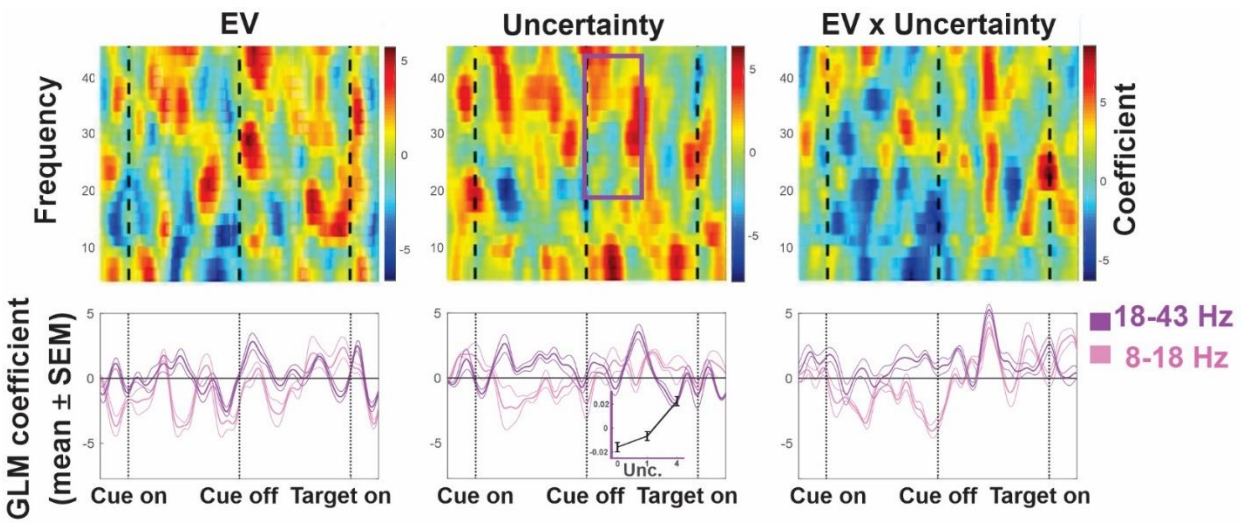

Figure S2. **LFP-LFP coherence. Uncertainty enhances oscillatory coherence in the higher frequency bands.**

The degree to which two areas synchronize their oscillations is a sensitive index of neural connectivity. We therefore tested whether, and how, the coherence of oscillations between frontal and parietal LFPs was affected by uncertainty and EV. In every session, for different time and frequencies (1 ms time bins and 2 Hz frequency bins), Weighted Phase Lag Index (WPLI; debiased WPLI option in the *ft_connectivityanalysis()* function of the FieldTrip toolbox) of LFP was calculated across trials and all electrode pairs between dlPFC and 7A. GLM with factors of EV, uncertainty and their interaction was then fitted to the coherence maps from different sessions, assuming normal distribution and identity link function. The LFP synchrony in the high-β/low-γ frequency band (coefficient maps in **Fig. S2,** middle column, second row, purple time trace, all the conventions as in **Fig 3**) was consistently enhanced by uncertainty, with the strongest effect appearing during the 200 ms early delay epoch. The inset shows average coherence across sessions in the marked ROI for different levels of uncertainty (mean±SEM across sessions and p value from the Kruskal-Wallis test: monkey 1 var_0 = -0.047±0.0046, var_4 = -0.004±0.0048, p = 2.7×10^{-10}; monkey 2 var_0 = -0.024±0.0073, var_4 = 0.002±0.0062, p = 1.8×10^{-14}).